Hindawi
Mathematical Problems in Engineering
Volume 2021, Article ID 5541052, 7 pages
https://doi.org/10.1155/2021/5541052

Research Article

Study on the Dynamic Performance of Locally Resonant Plates with Elastic Unit Cell Edges

Yonggan Sun

School of Shipping and Naval Architecture, Chongqing Jiaotong University, Chongqing 400074, China

Correspondence should be addressed to Yonggan Sun; sunygqj@163.com

Received 15 February 2021; Accepted 26 May 2021; Published 7 June 2021

Academic Editor: Ji Wang

A Floquet–Bloch approach is employed to demonstrate the stop bands for an infinite locally resonant plate. In addition, the effects of the connection stiffness of the unit cells on the band gap and dynamic performance of a locally resonant plate are analysed. The results show that the degree of inhibition of elastic waves in the band gaps increases rapidly when the connection stiffness of the unit cells increases within the scope of the transition stage stiffness. However, outside of the range of transition stage stiffness, the degree of inhibition of elastic waves in the band gaps basically remains unchanged. This discovery widens the application scope for vibration and noise control using locally resonant plates.

1. Introduction

The dynamic and vibrational properties of various structures have always been a topic of interest to scholars [1-7]. Periodic structures have attracted a great deal of attention in the field of vibration and noise control due to their unique physical properties and wave propagation characteristics. Elastic wave propagation in periodic structures decays rapidly within a certain frequency range, which is known as the band-gap frequency, and the other frequency range is known as the pass-band frequency. Generally, band gap generation conditions are divided into two categories: Bragg scattering mechanisms and locally resonant theory [8]. The length of the elastic wave that corresponds to the band-gap frequency based on the Bragg scattering mechanism is always of the same order as the lattice size, so the band gap generally occurs within the high-frequency range. At the same time, the length of the elastic wave that corresponds to the band-gap frequency based on locally resonant band gap theory is longer than the lattice size, so a low-frequency band gap can be obtained. This phenomenon has attracted significant attention from researchers, both domestically and overseas.

The locally resonant plate is suitable for vibration and noise control within different frequency ranges and has strong vibration and noise absorption ability in a narrow frequency range. However, typical narrowband properties hinder the application of locally resonant plates. To expand applicability, domestic and overseas scholars have proposed various strategies for the expansion of the band-gap frequency range of locally resonant plates. Peng et al. [9, 10] studied the working mechanism and design criteria for the modelling technology of single and multiple band-gap plates and noted that the band-gap frequency can be widened by increasing the mass of the unit cell, which is not conducive to light structure design. Casadei et al. [11] arranged resistance induction (RL) piezoelectric patches on an elastic plate periodically, and all shunting circuits were tuned to the same frequency. The results showed that structural acoustic radiation in the band-gap frequency can be significantly inhibited, but only a very narrow band gap was obtained. Mei et al. [12] designed a thin-film acoustic locally resonant plate for the effective absorption of low-frequency noise in air. Claeys et al. [13] used Nastran and LMS Virtual Lab commercial software to calculate the acoustic radiation performance of a single band gap locally resonant plate, and the influence of the coincidence frequency and band-gap frequency on the acoustic radiation performance of a locally resonant plate was discussed. From the literature, it is found that all studies are carried out assuming a whole plate/membrane structure that is equivalent to rigid unit cell edges.

However, there are many examples of elastic coupled plates in practical engineering, for example, ship hulls, land and space vehicles, and building structures. To the best of the author's knowledge, there has been no work reported on the dynamic performance of locally resonant plates considering the effects of elastic unit cell edges. The main purpose of this study is to partially fill this research gap. The dynamic performance and vibration transfer performance of elastically coupled unit cells are of interest to both researchers and application engineers. An emerging understanding of the interactions of elastically coupled unit cells will provide insight into the utilization of these locally resonant plates in practical vibration control applications. This work will focus on the effects of the connection stiffness of unit cells on the band gap and vibration transfer performance of locally resonant plates.

This study is presented in four sections. Following the introduction, Section 2 provides the theoretical background for locally resonant plates based on a unit cell with an elastic connection, and the dispersion curves are obtained. In Section 3, the effects of elastic connection stiffness on the band gap and vibration transfer performance of the locally resonant plate are discussed. The final section presents a brief summary and the conclusions of the present investigations.

2. Theory

The locally resonant plate with elastic unit cell edges is shown in Figure 1. k_{cx}, k_{cy}, and k_{cz} are the x, y and z directional support connection stiffness coefficients, and k_{cr} is the rotation connection stiffness coefficient of the unit cell. In Figure 2, the degrees of freedom of unit cells are divided into three parts: the degrees of freedom inside a unit cell, the degrees of freedom of the boundary, and the degrees of freedom at the intersection of the boundary. According to the Floquet–Bloch theorem [14, 15], nodal displacement and nodal force on the boundary can be expressed as follows [16]:where $\mu_x = k_x L_x$ and $\mu_y = k_y L_y$ represent the x and y directional wave propagation constants, respectively, and the subscripts $(\mathrm{LB}, \mathrm{RB}, \mathrm{LT}, \mathrm{RT})$ and (L, R, B, T) represent the degrees of freedom at the intersections and the boundary degrees of freedom, respectively.

$$\begin{aligned}
U_R &= e^{-ik_x L_x} U_L,\\
U_T &= e^{-ik_y L_y} U_B,\\
F_R &= -e^{-ik_x L_x} F_L,\\
F_T &= -e^{-ik_y L_y} F_B,\\
U_{\mathrm{RB}} &= e^{-ik_x L_x} U_{\mathrm{LB}},\\
U_{\mathrm{LT}} &= e^{-ik_y L_y} U_{\mathrm{LB}},\\
U_{\mathrm{RT}} &= e^{-i\left(k_x L_x + k_y L_y\right)} U_{\mathrm{LB}},\\
F_{\mathrm{RB}} &= -e^{-ik_x L_x} F_{\mathrm{LB}},\\
F_{\mathrm{LT}} &= -e^{-ik_y L_y} F_{\mathrm{LB}},\\
F_{\mathrm{RT}} &= e^{-i\left(k_x L_x + k_y L_y\right)} F_{\mathrm{LB}},
\end{aligned} \tag{1}$$

With no consideration of the damping effect, the motion equation of the periodic unit cell under the excitation of a harmonic force is expressed in the following matrix form [17]:

$$\left([K] + [K_b] - \omega^2 [M]\right)\{U\} = \{F\}, \tag{2}$$

where $[K]$ and $[M]$ are the element stiffness matrix and mass matrix of the unit cells, respectively, and $[K_b]$ is the connection stiffness matrix of the unit cells, including k_x, k_y, k_z, and k_r. ω is the vibration circle frequency. $\{U\} = \{U_{LB}\ U_{LT}\ U_{RT}\ U_{RB}\ U_L\ U_R\ U_B\ U_T\ U_I\}^T$ is the displacement vector of the unit cells. The displacement vector is comprised of two parts: boundary displacement and internal displacement of the unit cell, and $\{F\} = \{F_{LB}\ F_{LT}\ F_{RT}\ F_{RB}\ F_L\ F_R\ F_B\ F_T\ F_I\}^T$ is the load vector. When waves travel freely, $\{F_I\} = 0$, and the left multiplication reduction matrix T and the displacement vector of the unit cell $\{U\}$ are represented by the most reduced displacement matrix $[U^*]$ [18]:

$$[U] = [T][U^*], \tag{3}$$

$$[F] = [R][F^*], \tag{4}$$

where $[U^*] = [U_{LB}\ U_L\ U_B\ U_I]$, $[F^*] = [F_{LB}\ F_L\ F_B\ F_I]$. Equations (3) and (4) are substituted into equation (2) and expressed as follows:

$$T^H\left([K] + [K_b] - \omega^2 [M]\right)T[U^*] = 0, \tag{5}$$

where T^H is the conjugate transpose matrix of T, and equation (5) can be given as follows [16]:

$$\left([K'] - \omega^2 [M']\right)[U^*] = 0. \tag{6}$$

Equation (6) is the eigenvalue equation of the frequency ω^2, and the frequency is expressed as the periodic function of μ_x and μ_y. For (μ_x, μ_y) and $(\mu_x + 2m_1\pi, \mu_y + 2m_2\pi)$, where m_1, m_2 are integers, the eigenvalue and the eigenvector obtained from equation (6) is the same. μ_x and μ_y are generally complex numbers. The real part represents the phase variation during wave propagation, while the imaginary part represents the wave attenuation along x and y directions of wave propagation. When μ_x and μ_y are the real values, the value given by equation (6) is real and positive, and the dispersion relation of the periodic structure can be solved. The curve for the characteristic frequencies varies with μ_x and μ_y and produces the dispersion diagram, which is the pass band of the periodic structure. Other frequency bands that have no characteristic frequency for μ_x and μ_y are the band gaps. If $\mathrm{Re}(\mu_x) \in [-\pi, \pi]$ and $\mathrm{Re}(\mu_y) \in [-\pi, \pi]$, the frequencies of the locally resonant plate can be obtained for the entire period range. When the structural material is isotropic, the wave propagates in a similar way in the positive or negative direction. The dispersion diagram of the unit cell is symmetric about $\mu_x = 0$ and $\mu_y = 0$, so the range of the wave propagation constant can be set as $\mathrm{Re}(\mu_x) \in [0, \pi]$ and $\mathrm{Re}(\mu_y) \in [0, \pi]$ [19].

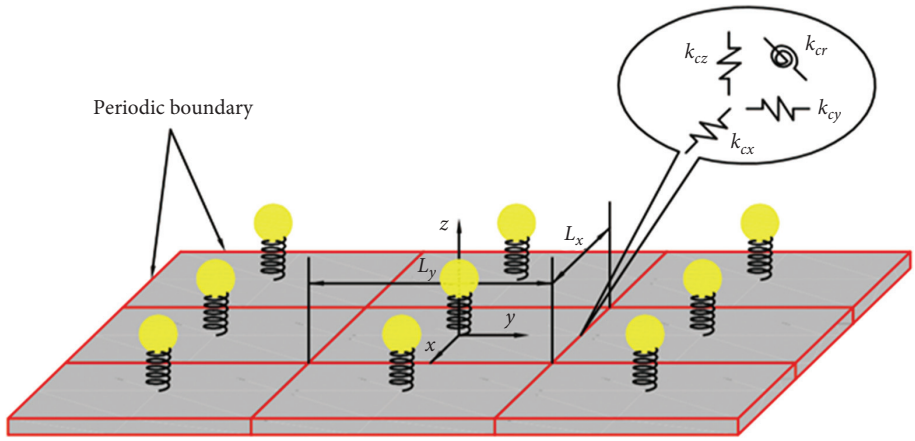

Figure 1: Schematic view of an infinite locally resonant plate.

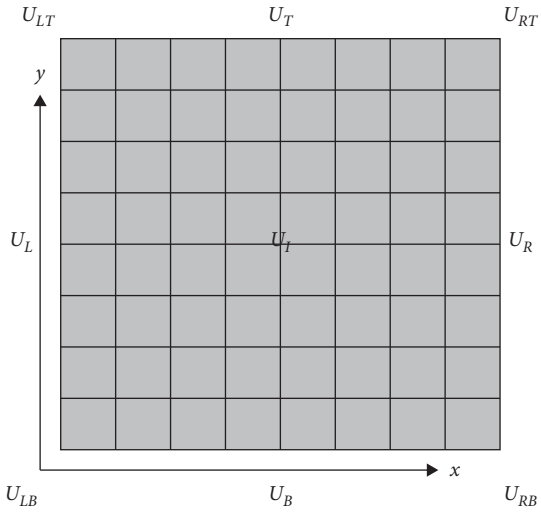

Figure 2: Definitions of the elements and nodes for a unit cell.

3. Numerical Results and Discussion

The unit cell of the locally resonant plate in this section is composed of a plate and a mass spring system, as shown in Figure 1, where the added mass is 20% of the base plate mass, and the spring stiffness is defined as follows [13]:

$$\frac{1}{2\pi}\sqrt{\frac{k}{m}} = p. \tag{7}$$

The material properties of the locally resonant plate are given in Table 1. The dispersion surface of the locally resonant plate is shown in Figure 3, assuming that the support connection stiffness coefficients and rotation connection stiffness coefficient of the unit cell are infinite, i.e., $k_{cx} = k_{cy} = k_{cz} = 1 \times 10^{15}$ Pa and $k_{cr} = 1 \times 10^{15}$ N/rad. The figure shows that the band-gap frequency of the locally resonant plate is 991 Hz–1092 Hz. The influence of the connection stiffness on the band-gap performance of the locally resonant plates will be discussed.

Assuming that the support connection stiffness coefficients k_{cx} and k_{cy} and rotation connection stiffness coefficient k_{cr} are infinite, i.e., $k_{cx} = k_{cy} = 1 \times 10^{15}$ Pa and $k_{cr} = 1 \times 10^{15}$ N/rad, the variation in band gap with boundary support connection stiffness coefficient k_{cz} is shown in Figure 4. The band-gap frequency range of the locally resonant plate is approximately 988 Hz–1000 Hz when the connection support stiffness coefficient of the locally resonant plate changes from 0 to 1×10^6 Pa (stage I). The band-gap frequency range of the locally resonant plate increases rapidly when the support connection stiffness coefficient of the unit cells increases from 1×10^6 Pa to 1×10^8 Pa (stage II, namely, the transition stage). The band-gap frequency range of the locally resonant plate basically remains unchanged (approximately 991 Hz–1092 Hz) when the support connection stiffness coefficient of the unit cells is greater than 1×10^8 Pa (stage III).

Figure 5 shows the variation in the band gap with the rotation connection stiffness coefficient k_{cr}, assuming that the connection stiffness coefficients are infinite, i.e., $k_{cx} = k_{cy} = k_{cz} = 1 \times 10^{15}$ Pa. The band-gap frequency range of the locally resonant plate basically remains unchanged (approximately 991 Hz–1018 Hz) when the boundary rotation connection stiffness coefficient increases from 0 to 1×10^4 N/rad (stage I). The band-gap frequency range of the locally resonant plate increases rapidly when the rotation connection stiffness coefficient increases from 1×10^4 N/rad to 1×10^6 N/rad (stage II, namely, the transition stage), and when the boundary rotation connection stiffness coefficient is greater than 1×10^6 N/rad, the band-gap frequency range of the locally resonant plate remains basically unchanged (stage III). At the same time, the lower limit of the band-gap frequency remains basically unchanged. Through a comparison of Figure 4 and Figure 5, it can be observed that the support connection stiffness coefficient has a greater influence on the band-gap frequency of the locally resonant plate than the boundary rotation connection stiffness coefficients.

The internal physical mechanisms for these phenomena can be interpreted as follows: the small connection stiffness coefficients actually lead to weak coupling of the unit cells, reducing the interaction of the resonators and the original

Table 1: Material properties and dimensions of the unit cell.

Density	$\rho_s = 7850\,\text{kg/m}^3$
Poisson's ratio	$v_s = 0.3$
Elasticity modulus	$E_s = 210\,\text{GPa}$
Thickness	$t_s = 15\,\text{mm}$
The size of unit cell	$L_x = L_y = 0.1\,\text{m}$

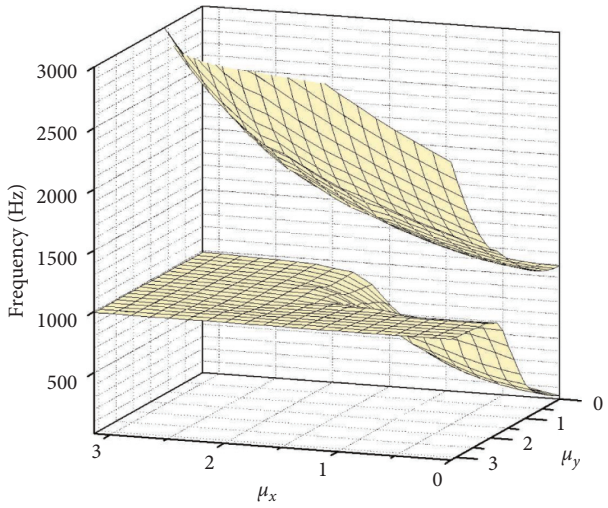

Figure 3: Dispersion surfaces for a locally resonant plate.

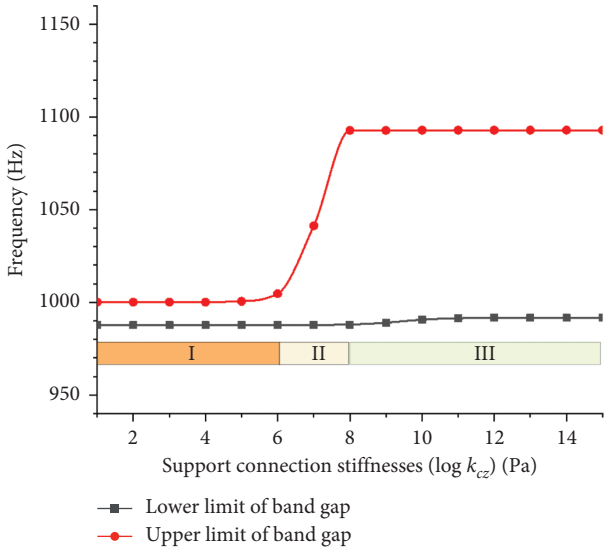

Figure 4: The band-gap frequencies of the locally resonant plate vary with different support connection stiffness coefficients of the unit cell.

structure to a certain degree, and the large connection stiffness coefficients lead to a high structural coupling of the unit cells, resulting in no free wave propagation, which is possible in a frequency region around the resonance frequency of the mass spring system.

In this study, a finite plate is derived by repeating the unit cell 10×10 times, so that a plate with dimension of 1 m by 1 m is obtained. The plate is simply supported along its

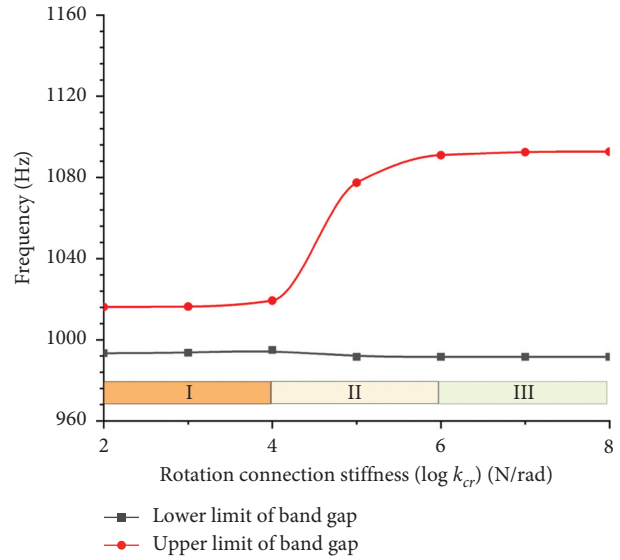

Figure 5: The band-gap frequencies of the locally resonant plate vary with different rotation connection stiffness coefficients of the unit cell.

boundaries, and the coordinate system is chosen as shown in Figure 1, $k_{cx} = k_{cy} = 1 \times 10^{15}$ Pa and $k_{cr} = 1 \times 10^{15}$ N/rad. When the support connection stiffness coefficient k_{cz} has different values and the unit harmonic force is applied along the z direction at (0.45 m, 0) of the finite locally resonant plate, the frequency response curve is obtained as shown in Figure 6. It can be observed from this figure that the velocity amplitude of the locally resonant plate slightly decreases within the band-gap frequency range and that the band gap is narrow when the support connection stiffness coefficient is $k_{cz} = 1 \times 10^7$ Pa. The velocity amplitude of the locally resonant plate within the band-gap frequency range significantly decreases and the width of the band-gap frequency range significantly increases when the boundary support connection stiffness coefficient of the unit cells is $k_{cz} = 1 \times 10^8$ Pa. When $k_{cz} = 1 \times 10^9$ Pa and $k_{cz} = 1 \times 10^{15}$ Pa, the velocity amplitude reduction of the locally resonant plate within the band-gap frequency range is almost the same. Figure 7 illustrates the frequency response curves for the locally resonant plate with different rotation connection stiffness coefficients for the unit cells. It has almost less effect on the frequency response of the locally resonant plate when the rotation connection stiffness coefficient is $k_{cr} = 5 \times 10^4$ N/rad. As the rotational stiffness coefficient further increases, a sensitive effect zone can be observed, in which increasing the connection stiffness coefficient of the unit cells will result in a large attenuation of the velocity amplitude over a wide range. When the connection stiffness coefficient increases beyond $k_{cr} = 1 \times 10^7$ N/rad, the velocity amplitude attenuation and width of the band-gap frequency range are basically unchanged, and most of the vibration energy is absorbed by the mass spring system in the band-gap frequency range, resulting in significantly low vibration amplitudes for the base plate structure. The vibration amplitudes of the finite locally resonant plate in response to excitations within the

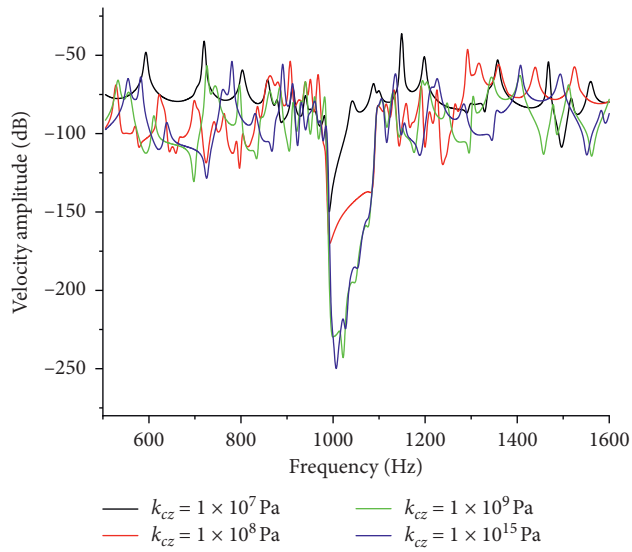

Figure 6: Frequency response curves for the locally resonant band-gap plate with different support connection stiffness coefficients of the unit cell.

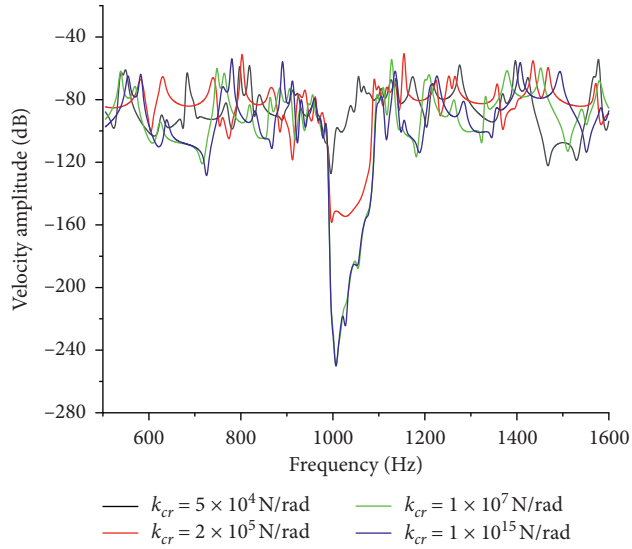

Figure 7: Frequency response curves for the locally resonant band-gap plate with different rotation connection stiffness coefficients of the unit cell.

pass-band frequencies are displayed in comparison and are significantly larger in magnitude. In summary, whether the support stiffness is increased or the rotation stiffness is increased, the higher limit of the band gap is affected the most by the connection stiffness coefficients, although the lower limit of the stop band remains mostly unchanged. In other words, the lower limit of the stop band is strongly linked to the resonance frequency of the mass spring system, while the upper limit is more influenced by the interaction of the mass spring system and the original plate structure with different connection stiffness coefficients.

The effect of connection stiffness coefficients on the vibration transfer function of the locally resonant plate can be shown by taking the rotation connection stiffness coefficient k_{cr} as an example. Assuming that the boundary support connection stiffness coefficients along the x, y, z directions are infinite, a unit harmonic force is applied at (0.45 m, 0) along the z direction at 1000.5 Hz frequency within the band gap. The variation in the velocity amplitude distribution of the locally resonant plate with the rotation connection stiffness coefficient k_{cr} is shown in Figure 8. It can be observed from this figure that the velocity amplitude distribution of the locally resonant plate is significantly reduced after seven unit cell periods when $k_{cr} = 5 \times 10^4$ N/rad. However, the velocity amplitude distribution of the locally resonant plate is significantly reduced after three unit cell periods when $k_{cr} = 2 \times 10^5$ N/rad. The velocity amplitude distribution of the locally resonant plate is significantly reduced after two unit cell periods when the rotation connection stiffness coefficient $k_{cr} = 1 \times 10^7$ N/rad,

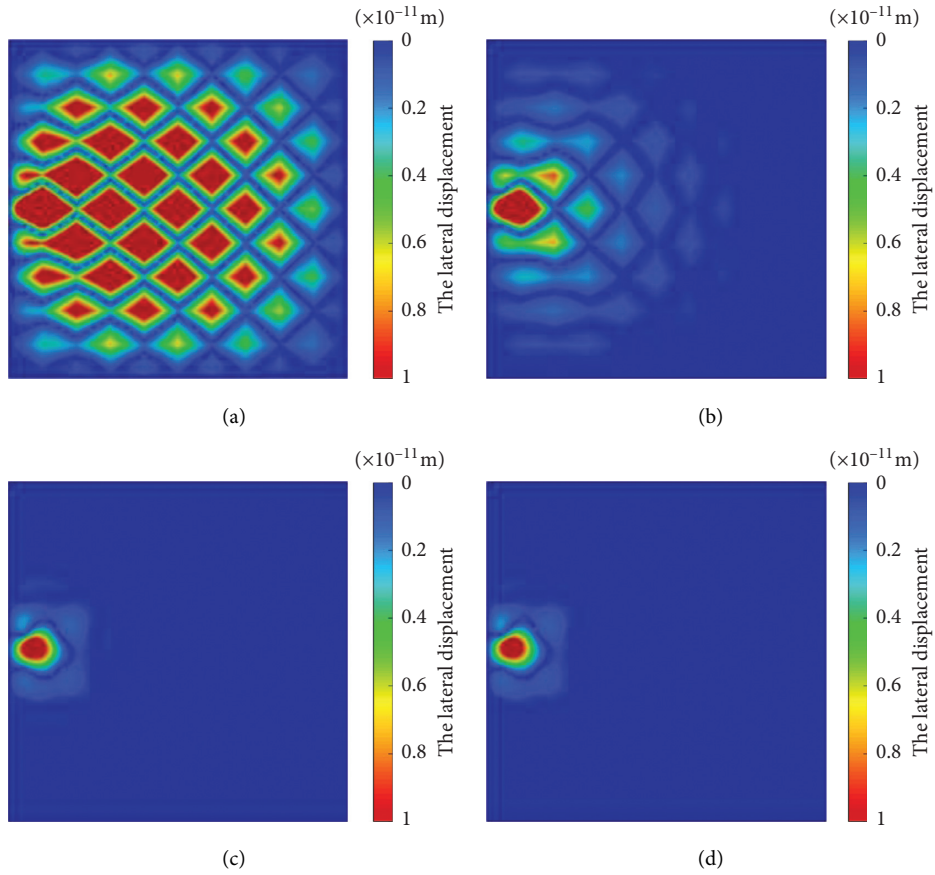

Figure 8: The velocity amplitude distribution of the locally resonant plate (z direction). (a) $k_{cr} = 5 \times 10^4$ N/rad. (b) $k_{cr} = 2 \times 10^5$ N/rad. (c) $k_{cr} = 1 \times 10^7$ N/rad. (d) $k_{cr} = 1 \times 10^{15}$ N/rad.

and when $k_{cr} = 1 \times 10^7$ N/rad and $k_{cr} = 1 \times 10^{15}$ N/rad (stage III), the velocity amplitude distribution of the locally resonant plate basically remains the same.

The above discussion proves that there exists a "transition stage stiffness" for the unit cell, within which the band gap and the degree of inhibition of elastic waves increase rapidly when the connection stiffness coefficients of the unit cells increase. Outside of the transition stage stiffness range, the band gap and the degree of inhibition of elastic waves basically remain unchanged.

4. Conclusions

In this study, a computational model of a locally resonant plate based on the elastic connection of unit cells was established, and the influence of connection stiffness coefficients on the band gap and vibration performance of a local resonant structure was analysed. It was found that the band gaps can be tuned using the connection stiffness of the unit cells, and the bandwidth and degree of inhibition increase rapidly in the range of the transition stage stiffness. The effect of vibration reduction of local resonant structures is not affected if the corresponding connection stiffness coefficients are adjusted above the transition stage. This new discovery is of great significance to the practical application of local resonance plates in vibration and noise control.

Data Availability

The data generated or analysed to support the findings of this study are included within the article.

Conflicts of Interest

The authors declare that there are no conflicts of interest.

Acknowledgments

This project was supported by the Scientific and Technological Research Program of Chongqing Municipal Education Commission (KJQN201800726).

References

[1] N. Bendenia, M. Zidour, A. A. Bousahla et al., "Deflections, stresses and free vibration studies of FG-CNT reinforced sandwich plates resting on Pasternak elastic foundation," *Computers and Concrete*, vol. 26, no. 3, pp. 213–226, 2020.

[2] A. Menasria, K. Abdelhakim, A. A. Bousahla et al., "A four-unknown refined plate theory for dynamic analysis of FG-sandwich plates under various boundary conditions," *Steel and Composite Structures*, vol. 36, no. 3, pp. 355–367, 2020.

[3] O. Allam, K. Draiche, A. A. Bousahla et al., "A generalized 4-unknown refined theory for bending and free vibration

analysis of laminated composite and sandwich plates and shells," *Computers and Concrete*, vol. 26, no. 2, pp. 185–201, 2020.

[4] M. C. Rahmani, K. Abdelhakim, A. A. Bousahla et al., "Influence of boundary conditions on the bending and free vibration behavior of FGM sandwich plates using a four-unknown refined integral plate theory," *Computers and Concrete*, vol. 25, no. 3, pp. 225–244, 2020.

[5] M. Rabhi, K. H. Benrahou, K. Abdelhakim et al., "A new innovative 3-unknowns HSDT for buckling and free vibration of exponentially graded sandwich plates resting on elastic foundations under various boundary conditions," *Geomechanics and Engineering*, vol. 22, no. 2, pp. 119–132, 2020.

[6] M. Al-Furjan, A. Hatami, M. Habibi et al., "On the vibrations of the imperfect sandwich higher-order disk with a lactic core using generalize differential quadrature method," *Composite Structures*, vol. 257, Article ID 113150, 2021.

[7] H. Hirane, M. O. Belarbi, M. Houari et al., "On the layerwise finite element formulation for static and free vibration analysis of functionally graded sandwich plates," *Engineering with Computers*, 2021.

[8] M.-H. Lu, L. Feng, and Y.-F. Chen, "Phononic crystals and acoustic metamaterials," *Materials Today*, vol. 12, no. 12, pp. 34–42, 2009.

[9] H. Peng and P. Frank Pai, "Acoustic metamaterial plates for elastic wave absorption and structural vibration suppression," *International Journal of Mechanical Sciences*, vol. 89, pp. 350–361, 2014.

[10] P. Hao, P. F. Pai, and H. Deng, "Acoustic multi-stopband metamaterial plates design for broadband elastic wave absorption and vibration suppression," *International Journal of Mechanical Sciences*, vol. 103, pp. 104–114, 2015.

[11] F. Casadei, L. Dozio, M. Ruzzene, and K. A. Cunefare, "Periodic shunted arrays for the control of noise radiation in an enclosure," *Journal of Sound and Vibration*, vol. 329, no. 18, pp. 3632–3646, 2010.

[12] J. Mei, G. Ma, M. Yang, Z. Yang, W. Wen, and P. Sheng, "Dark acoustic metamaterials as super absorbers for low-frequency sound," *Nature Communications*, vol. 3, no. 1, p. 756, 2012.

[13] C. C. Claeys, P. Sas, and W. Desmet, "On the acoustic radiation efficiency of local resonance based stop band materials," *Journal of Sound and Vibration*, vol. 333, no. 14, pp. 3203–3213, 2014.

[14] F. Farzbod and M. J. Leamy, "The treatment of forces in Bloch analysis," *Journal of Sound and Vibration*, vol. 325, no. 3, pp. 545–551, 2009.

[15] F. Farzbod and M. J. Leamy, "Analysis of Bloch's method and the propagation technique in periodic structures," *Journal of vibration and Acoustics*, vol. 133, no. 3, Article ID 031010, 2011.

[16] M. A. Nouh, O. J. Aldraihem, and A. Baz, "Periodic metamaterial plates with smart tunable local resonators," *Journal of Intelligent Material Systems and Structures*, vol. 27, no. 13, pp. 1829–1845, 2015.

[17] O. Chiello, F. Sgard, and N. Atalla, "On the use of a component mode synthesis technique to investigate the effects of elastic boundary conditions on the transmission loss of baffled plates," *Computers and Structures*, vol. 81, no. 28-29, pp. 2645–2658, 2003.

[18] T. U. R. Abbasi and H. Zheng, "Wave dispersion and dissipation performance of locally resonant acoustic metamaterials using an internal variable model," *Wave Motion*, vol. 93, Article ID 102483, 2020.

[19] B. R. Mace and E. Manconi, "Modelling wave propagation in two-dimensional structures using finite element analysis," *Journal of Sound and Vibration*, vol. 318, no. 4, pp. 884–902, 2008.